EXPERIMENTAL SIMULATION OF A GALILEO SUB-SCALE MODEL AT ICE GIANT ENTRY CONDITIONS IN THE T6 FREE-PISTON DRIVEN WIND TUNNEL

Joseph Steer[1], Peter Collen[1], Alex Glenn[1], Tamara Sopek[1], Christopher Hambidge[1], Luke Doherty[1], Matthew McGilvray[1], Stefan Loehle[2], and Louis Walpot[3]

[1]*Oxford Thermofluids Institute, University of Oxford, Oxford, UK*
[2]*High Enthalpy Flow Diagnostics Group (HEFDiG), Institute of Space Systems (IRS), Stuttgart, Germany*
[3]*ESA/ESTEC, Keplerlaan Noordwijk, The Netherlands*

ABSTRACT

Uranus and Neptune, known collectively as the Ice Giants, are the only two planets in the solar system that are yet to be explored with a dedicated mission. Planetary entry probe missions to the Ice Giants were proposed in 2010 by NASA and ESA which prompted a resurgence of interest in experimental simulation of the aeroheating environment that would be encountered by such a spacecraft. More recently, the 2023 - 2032 Decadal Survey recommended that NASA's highest priority new flagship mission should be a Uranus orbiter and probe with a launch date in the early 2030s. The Oxford T6 Stalker tunnel is the only facility in Europe capable of replicating the high speeds required for Ice Giant entry and is therefore a key stepping stone on the path to realising the goal of an Ice Giant mission. In the present work, a 1:10 scaled model of the Galileo probe has been tested at Ice Giant entry conditions. Conditions for nominal composition (85%$H_2$15%He), Stalker substituted, and nominal composition with methane (0.5% and 5% CH_4) gas mixtures have been developed and validated for use with a new expansion nozzle via a pitot rake survey. Test flows with flight equivalent velocities greater than 18 km/s have been produced with test times on the order of 30 μs. Heat flux into the model for the developed conditions has been inferred from temperature measurements with a series of coaxial thermocouples. High speed video has been captured to aid in characterisation of the test conditions.

Key words: high enthalpy; expansion tunnel; ice giants.

1. INTRODUCTION

The Ice Giants represent a class of planets in our solar systems that are the least understood but the most frequently observed type of exoplanet [1]. Our knowledge of atmospheric processes occurring on these planets and thus their role in the evolution of the solar system is primarily derived from Earth based telescopes which are associated with a high level of uncertainty. This uncertainty motivates the design of an atmospheric probe mission, identified as a high priority by NASA and ESA on multiple occasions [2, 3], most recently in the 2023 - 2032 Decadal Survey [4]. Such a probe would encounter an extreme heating environment on entry to the hydrogen/helium atmosphere, comparable perhaps only to the Galileo probe entry to Jupiter in 1995 [5]. These extreme conditions demand that a comprehensive ground testing program accompany the design of the entry module, which T6 is well placed to contribute to as the only facility in Europe capable of replicating the high speeds required for Ice Giant entry [6, 7] in expansion tube, expansion tunnel, and shock tube modes.

The field of Gas Giant entry research might be divided into two periods: a Galileo related period from 1960s - 2000s and a post decadal survey period from 2010 - present day. This distinction is fitting because of the time difference and because of the large difference in entry conditions and therefore total heat flux between Jupiter trajectories and the other gas planets, as shown in Table 1. Gas Giant entry research began with design and analysis of the Galileo probe [8], and subsequent analysis was conducted after the capsule entry with a focus on replicating the observed heat shield recession numerically [9, 10]. The Uranus and Neptune entry trajectories proposed by ESA [2] and the expected aeroheating uncertainty for these entries were analysed by Palmer et al. in [11]. Radiation for these trajectories was simulated experimentally by Cruden et al. [12] in the Electric Arc Shock Tube (EAST) at NASA Ames Research Center.

Table 1: Typically quoted values for entry velocity and stagnation enthalpy for gas planet trajectories

Planet	**Jupiter**	**Saturn**	**Uranus/Neptune**
v [km/s]	47	26.9	22.3
h_{stag} [MJ/kg]	1,130	362	249

The use of expansion tubes to experimentally simulate Gas Giant entry has been explored by James et al. [13] and Liu et al. [14] at the X2 facility at the University of Queensland. These efforts have made use of a test

gas substitution or Stalker substitution, first proposed by Ray Stalker in 1980 [15]. The substitution is a method for achieving an aerothermodynamically similar environment to Gas Giant entry with less energy addition than would otherwise be required. The test gas, roughly 85%$H_2$15%He for Gas Giant entry, is modified with a higher percentage of He or Ne. With higher percentages of He or Ne the total specific heat of the gas decreases, meaning that less energy addition is required to reach a given post-shock temperature. Stalker found that the type of diluent did not affect the post-shock relaxation process and postulated that this was because the diluent behaved as a third body or electron reservoir and did not react chemically. It was found that the substitution allowed the H_2 dissociation and ionization processes for Uranus and Saturn entry shock layers to be modelled in X2.

Although test gas substitution offers many advantages, it also has several limitations. One of the four requirements for validity of the blunt body flow similarity transformation that underpins the test gas substitution [16] is that variation of the post-shock density ratio (ϕ) along a streamline is the same for the two flows. Stalker and Edwards [17] showed that the nonequilibrium variation of the density ratio with a hydrogen binary reaction variable is independent of the type and amount of diluent used. However, they noted that because the equilibrium density varies with pressure, similarity is lost for flows at different pressure levels in equilibrium. This is a limitation of the scaling technique as it does not allow the full flow field chemistry to be modelled in a single experiment and it is therefore unclear if parameters of interest, especially surface heat flux, can be replicated between substituted conditions. Another underlying assumption is that the diluent (helium or neon) acts as an inert third body in any reactions. As neon has a much lower excitation energy than helium (17 eV vs 21 eV) and can ionise, this limits the conditions at which it can be used as a diluent.

Although significant progress in Gas Giant entry research has been made in the last ten years, many studies have neglected the influence of trace components such as CH_4 on the aeroheating environment. In a review paper, Moses et al. [18] summarise the observed abundance of tropospheric and stratospheric constituents on the Ice Giants. These values are reproduced in Tables 2 and 3.

Table 2: Tropospheric composition of the Ice Giants by volume from [18]

Species	Uranus	Neptune
He	15.2%	14.9%
CH_4	1.4 - 4%	2 - 5%
NH_3	30 - 90 ppm	40 - 200 ppm
H_2O	<5%	27%
PH_3	<2 ppm	<1.1 ppb at 0.7 bar
H_2S	0.4 - 0.8 ppm	1 - 3 ppm

From Titan entry experiments CH_4 is known to be a significant contributor to radiative heat flux. Recent work by Coelho [19] predicts that the presence of 1.5 % CH_4 significantly enhances the radiative heat flux for Ice Giant entry trajectories. Where Cruden et al. [12] found that radiative heating is negligible for speeds lower than 25 km/s, Coelho predicts that the presence of CH_4 means radiative heating becomes comparable to convective heating even for relatively low speeds of 18 km/s. The bulk of the deceleration and therefore aeroheating for Ice Giant trajectories is expected to occur in the stratosphere [3], where CH_4 abundance on Neptune is expected to be an order of magnitude lower than the value modelled by Coelho - abundance on Uranus is expected to be three orders of magnitude lower. Given that the Decadal Survey has identified a Uranus mission as the priority the requirement for detailed studies of surface heat flux with CH_4 mixtures is lessened. However, establishing this capability will still be informative for modelling of the atmosphere and heat shield recession post-flight as done by, for example, [20].

Table 3: Stratospheric composition of the Ice Giants by volume from [18]

Species	Uranus	Neptune
CH_4	16 ppm at 50 mbar	0.115% at 5 mbar
C_2H_2	0.25 ppm at 0.2 mbar	0.033 ppm at 0.5 mbar
C_2H_4	$<2 \times 10^{-14}$ at 10 mbar	0.8 ppb at 0.2 mbar
C_2H_6	0.13 ppm at 0.2 mbar	0.85 ppm at 0.3 mbar
C_3H_4	0.36 ppb at 0.4 mbar	0.12 ppb at 0.1 mbar
C_4H_2	0.13 ppb at 0.4 mbar	0.003 ppb at 0.1 mbar
CO_2	0.08 ppb at 0.14 mbar	0.78 ppm at 0.1 mbar
CO	6 ppb at 0.5 mbar	1.1 ppm at 0.1 mbar
H_2O	3.8 ppb at 0.03 mbar	2.5 ppm at 0.16 mbar
D/H	4.4×10^{-5}	4.1×10^{-5}

In the present work, a 1:10 scaled model of the Galileo probe has been tested at Ice Giant entry conditions proposed by ESA [3] as these are associated with a comprehensive numerical data set that can be used for comparison. The use of sub-scale models necessitate that test conditions are binary scaled [21, 22]. Binary scaling is a method that allows the flight shock layer to be duplicated in a wind tunnel in the vicinity of the shock layer. In a binary scaled experiment, the total enthalpy (essentially $\frac{U^2}{2}$) and the post bow shock ρL are matched to flight. This scaling replicates most of the desired properties from flight around the model, apart from radiation which does not scale directly [23].

The following section provides details of the T6 facility performance and a new expansion nozzle. The third section details the experimental arrangement, specifically descriptions of the Pitot rake and sub-scale vehicle. Results from initial testing are presented in the fourth section with possible future work following.

2. FACILITY DESCRIPTION

T6, as shown in Figure 1, is a multi-mode hypersonic wind tunnel. The free-piston driver, which generates pressures on the order of 50 MPa during a shot, may be coupled to a range of downstream components to allow operation of the facility as either a shock tube, expansion tube, expansion tunnel, or reflected shock tunnel. T6 offers the only expansion tube facility in Europe and the highest performing shock tube in Europe. Ice Giant experiments will be run in expansion tube/tunnel mode to replicate aerodynamic parameters and provide insight into the non-equilibrium thermochemistry occurring in the shock layer. A more detailed overview of T6 can be found in [24].

The expansion tube concept, first proposed by [25], offers the ability to significantly increase the total enthalpy of the flow at the cost of reducing test time. In an expansion tube, the test gas is initially processed by an incident shock followed by rupture of the primary diaphragm. A thin, secondary diaphragm separates the test gas from low pressure lab air which is ruptured on contact with the shock. The rupture of the secondary diaphragm allows the high-pressure, shock heated test gas to unsteadily expand into the acceleration tube, resulting in an increase in total enthalpy. The apparatus becomes an expansion tunnel when a nozzle is coupled with the acceleration tube with the goal of expanding the usable core flow diameter, allowing larger sub-scale models to be tested [26]. The design of such a nozzle for use with He/H mixtures has been completed specifically for this study.

The contour of the nozzle was scaled from the University of Queensland X2 nozzle to the larger inlet diameter of the T6 facility. This has an outlet diameter of 236 mm, producing core flows of 180 mm in diameter, with a nominal entry Mach number of 7.3 and exit Mach number of 10. Attachment points have been included at nozzle exit to allow for measurements of exit static pressure.

3. EXPERIMENTAL ARRANGEMENT

3.1. Pitot Rake Experiments

A Pitot rake was setup in the test section to record the nozzle outflow properties and thereby assess the suitability of the conditions for model testing. The rake has 11 slots spaced at regular 20 mm intervals to house type 113 PCB pressure transducers. The rake was located 20 mm downstream of the nozzle outlet and on the nozzle center line. A pressure transducer was also located at the nozzle exit plane in order to measure the static outlet pressure. More detailed information about the T6 pitot rake can be found in [6].

3.2. Sub-scale Vehicle Experiments

The design of the capsule model is based on dimensions of the Galileo spacecraft heat shield. The scaling of the model was determined primarily by the predicted nozzle core flow size of between 180 mm and 200 mm in diameter for Ice Giant test conditions. A planform diameter of 126 mm was selected, corresponding to a 1:10 scaling of the Galileo probe. The model has a nose radius of 22.2 mm (L in the ρ-L scaling parameter), a length of 90 mm. The model was machined from EN24 steel and was surface hardened to 60 HRC. To allow for mounting of the model in the T6 test section the backshell was not machined and the model was truncated at the end of the sphere-cone geometry. The model is pictured in the T6 test section in Figure 3.

The model is instrumented with both thermocouples to infer heat transfer and pressure transducers to infer angle of attack. Six K-type coaxial thermocouples from the Medtherm corporation were installed flush against the model surface at 10 mm intervals starting at the stagnation point. This type of thermocouple has a response time of approximately 1 μs and has been widely used in hypersonic ground test facilities. K-type sensors were selected so that the probe material would have values of the thermal diffusivity, α, and thermal conductivity, k, that matched the corresponding wall material value of $\sqrt{\rho c k}$ (or $k/\sqrt{\alpha}$) as nearly as possible. The sensors have an outer diameter of 0.061" (1.54 mm) and a tube length of 0.25" (6.35 mm). The manufacturer quoted sensitivity and thermal product of the sensors were 41 µV and 8665 $\mathrm{Jm^{-2}K^{-1}s^{-0.5}}$ respectively.

Two slightly different models of thermocouple were purchased, one where the negative junction was electrically isolated from the model surface (triaxial or revision A) and one where the negative junction was in contact. This was done in an effort to assess the effect of noise from the highly ionised flow environment on the thermocouple signal. It was quickly found that the electrically isolated models were far less noisy that the standard model and all standard model thermocouples were subsequently removed from the model and electrically isolated by applying heat shrink tube around the outer diameter.

Three PCB type 113 pressure transducers were installed with 120°azimuthal spacing. The surface of the PCBs was recessed by approximately 3 mm from the model surface to remove them from the flow line of sight and hence limit the chance of damage from diaphragm fragments entrained in the flow. A detailed summary of the model sensor layout is shown in Figure 2.

A Kirana high-speed camera was set up perpendicular to the flow plane as shown in figure 3 to record video of the test time. The frame rate was set between 1 million and 2 million FPS with an exposure time between 100 and 500 ns depending on the expected brightness of the condition. The settings allowed the time from 20 µs before

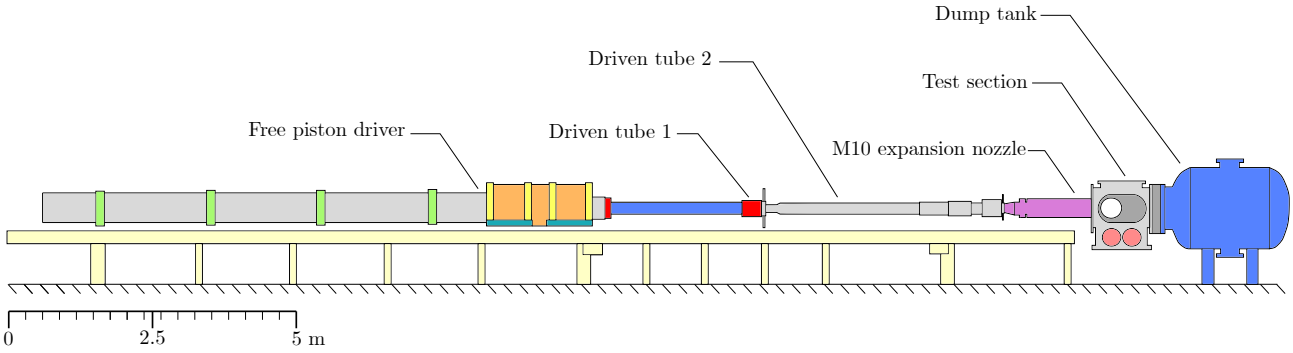

Figure 1: Schematic of the T6 facility in expansion tunnel mode, showing the arrangement of different components. In expansion tube mode, the expansion nozzle is replaced with a third driven tube.

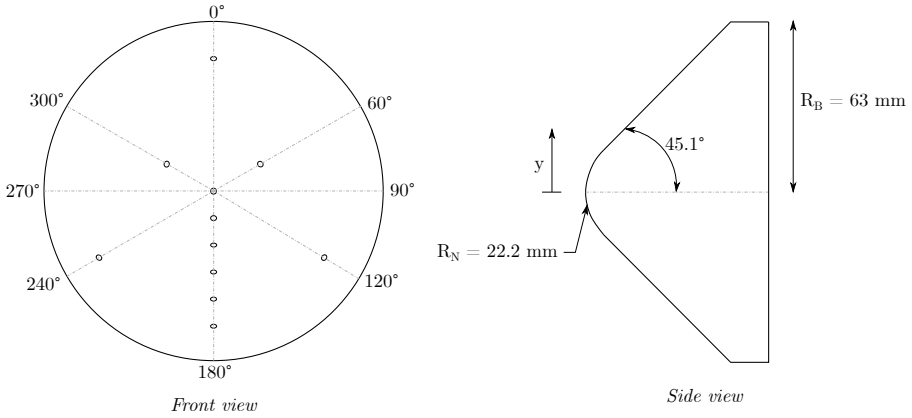

Figure 2: Schematic diagram of the instrumentation layout for the Galileo sub-scale model

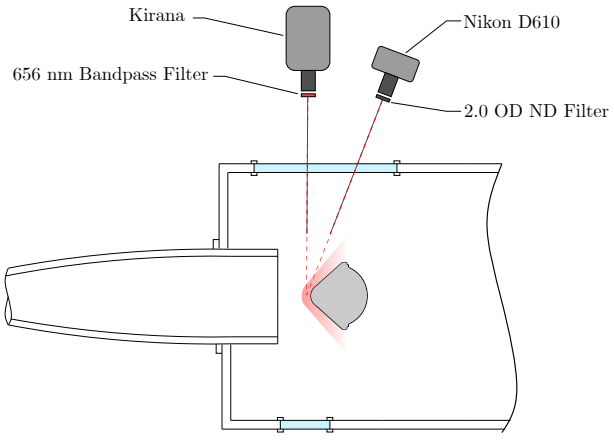

Figure 3: Schematic diagram of the optics setup used in initial gas giant entry experiments

flow arrival to 60 µs after to be captured which included arrival of the accelerator gas through to completion of the test time. For later tests, a 656 mm band pass filter was placed in front of the camera to isolate the H-α line.

4. TESTED CONDITIONS

4.1. Condition Details

Conditions for nominal composition (85%H_2 / 15%He), Stalker substituted, and nominal composition with methane (0.5% and 5% CH_4) gas mixtures have been developed and are detailed in Table 4. The shock tube and acceleration tube fill pressures, p_1 and p_5 respectively, were selected in order to maximise the total enthalpy of the test gas for condition A. The primary and secondary shock speeds, U_{s1} and U_{s2} respectively, were calculated using measurements from 9 shock timing stations distributed along the length of the facility. The freestream total enthalpy (H_0), density (ρ_∞), total temperature ($T_{t,\infty}$), and post-shock frozen temperature ($T_{10,f}$) have been calculated using PITOT [27].

Figure 4 shows the measured shock speeds for each condition. As expected, the maximum shock speed was observed for condition A where the largest fraction of H_2

Table 4: Summary of tested conditions

Condition	Test Gas Composition [%v/v]	p_1 [Pa]	p_5 [Pa]	U_{s1} [m/s]	$U_{s2/\infty}$ [m/s]	H_0 [MJ/kg]	ρ_∞ [kg/m3]	$T_{t,\infty}$ [K]	$T_{10,f}$ [K]
A	85%H_2 / 15%He	2362	2.2	8923	18397	176.3	9.67e-5	7262	14403
B	40%H_2 / 60%He	2614	2.5	8462	17146	153.7	1.83e-4	11458	19755
C	15%H_2 / 85%Ne	2334	2.5	7561	13954	105.0	1.34e-3	31045	32967
D	84.5%H_2 / 15%He / 0.5%CH_4	2548	2.5	8373	16392	141.8	1.57e-4	6257	35920

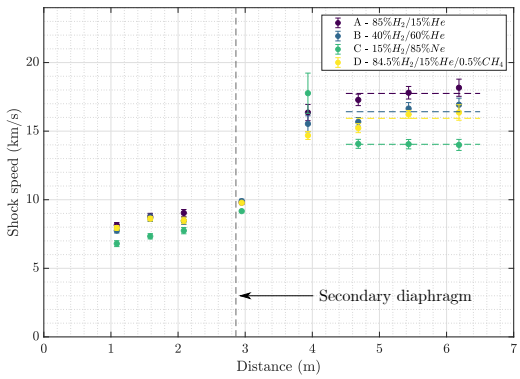

Figure 4: Comparison of shock speeds for tested conditions

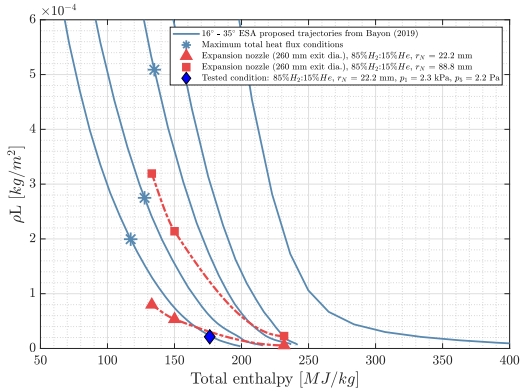

Figure 5: Plot of experimental conditions achieved versus ESA candidate Ice Giant entry trajectories

is present. A secondary shock speed of 18.39 $\mathrm{km\,s^{-1}}$ (corresponding to a flight equivalent velocity of 18.90 $\mathrm{km\,s^{-1}}$) was achieved.

Figure 5 shows a comparison of the achieved experimental performance for condition A versus several candidate Ice Giant entry trajectories proposed by ESA [3]. PITOT simulations tuned to experimental performance for the existing 'high' driver condition of 46.2 MPa, a test gas fill pressure of 2.3 kPa and a range of acceleration tube fill pressure between 10 and 0.5 Pa are also shown as an indicator of the achieveable performance. To simulate higher density trajectory points, an experimenter could increase the model size, run without an expansion nozzle which sacrifices core flow size, or increase the acceleration tube fill pressure which would decrease total enthalpy.

A wide parameter space is available to improve the facility total enthalpy performance. The minimum achievable acceleration tube fill pressure was limited by a high leak rate into the test section. Ultimate pressures of less than 1 mPa were achieved in a recent shock tube campaign without the test section installed, indicating that with sufficient effort these pressures could be achieved in expansion tunnel mode. The acceleration tube fill pressure is strongly related to the achieve able total enthalpy as shown in Figure 5. The use of thinner secondary diaphragm material could be explored to reduce losses. Thicknesses of 1 and 2 $\mu\mathrm{m}$ have been purchased but were avoided for the initial campaign due to their proclivity to tear. Finally, a new driver condition could be utilised. It is believed that losses through the primary diaphragm could be lessened by reducing the diaphragm opening time which would necessitate a different diaphragm material. Design of a more powerful driver condition is also possible, but may require manufacture of a lighter piston.

Higher enthalpy flight conditions could also be modelled by designing Stalker substituted test conditions as done by James et al. [28]. In such experiments, the scaling parameters become the post shock temperature and a modified binary scaling parameter to match the rate of hydrogen dissociation between conditions. The substitution breaks down if ionisation of the inert diluent (He or Ne) occurs which was the case for condition C in Table 4. However, the post shock frozen temperatures achieved for conditions C and D are a promising indicator that T6 is capable of achieving the required performance for Stalker substituted Saturn entry modelling (post shock frozen temperature $\approx$ 27,000 K) given appropriate condition design.

4.2. Pitot Rake Experiments

Figure 6 shows pitot pressure traces obtained over the test time for condition A and has been annotated with marks indicating the test time. The data indicate that the test time is 30 - 50 μs. Figure 7 shows the test time averaged pitot pressure for each sensor in the rake versus the radial location, 0 mm being the nozzle centerline. PP11 records a lower pressure than the others, indicating that it

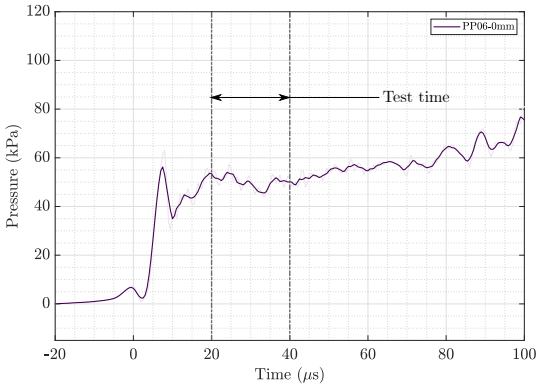

Figure 6: Pitot pressure traces for condition A

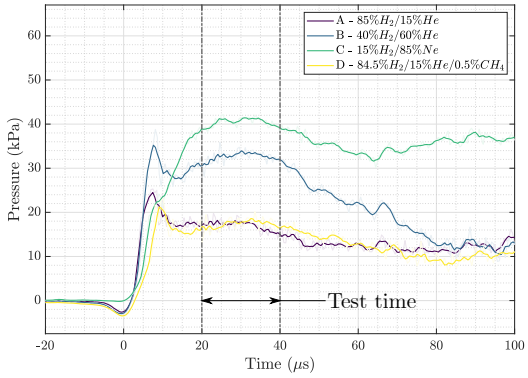

Figure 8: Model surface pressures

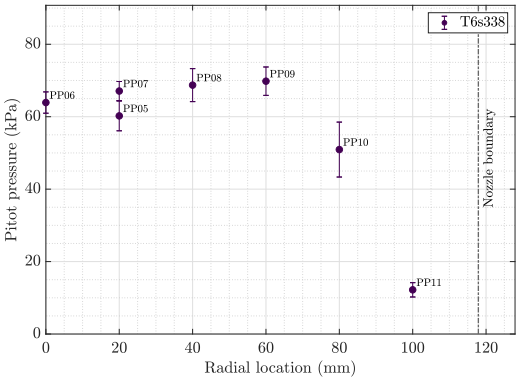

Figure 7: Test time averaged pitot pressures for condition A

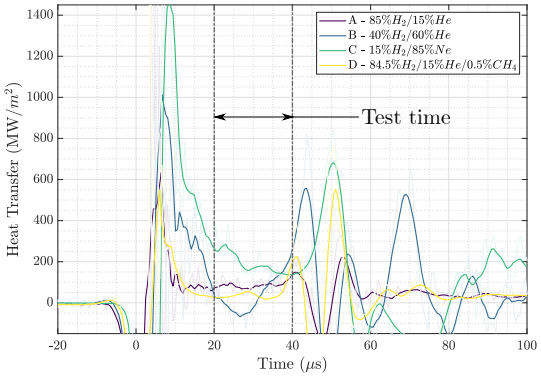

Figure 9: Model stagnation point heat transfer

is outside the nozzle core flow. Considering the geometry of the rake, this gives a core flow diameter of at least 160 mm. The uncertainty associated with each point in Figure 7 is simply one standard deviation of the measurements in the test time.

4.3. Sub-scale Vehicle Experiments

Figure 8 shows traces obtained from the pressure transducers installed in the model over the test time. Only one traces is shown for each condition as results were effectively equivalent between the three transducers. The response time of the PCBs does not appear to have been significantly reduced by the recessed mounting technique employed.

Heat flux was inferred from temperature change for each thermocouple using the inverse heat transfer technique for semi-infinite substrates detailed in [29]. Sensitivity of the thermocouples was assumed constant at 41 μV . K^{-1} and the thermal product was assumed constant at 8665 $J.m^{-2}.K^{-1}.s^{-0.5}$, although this has been shown to change over the course of the test time [30]. The temperature increase observed during the test time ranged between 50 - 100 K. All thermocouples were electrically isolated from the model.

Figure 9 shows processed heat transfer traces at the stagnation point for each test condition, the test time begins at 10 µs. Each of the traces is characterised by a large 'dip' just before flow arrival. This feature is almost certainly spurious and due to the highly ionised accelerator gas imparting a negative charge on the surface of the model and in turn the thermocouples. In general, the traces for conditions B and C were much noisier than conditions A and D. This may be because the test gas in conditions B and C was more ionised and therefore electrically noisy. The heat flux for condition B dips and becomes negative during the test time which is clearly non-physical. This could because the thermocouple was struck by a diaphragm fragment or other debris.

Figure 10 shows a plot of the test time averaged heat flux against the normalised surface distance to nose radius ratio for each thermocouple. The validity of the results is dubious given that for nearly every condition the average heat transfer was higher away from the stagnation point.

Table 5 shows the average stagnation point heat flux for each condition versus the corresponding Sutton & Graves convective prediction [31]. The correlation is of the form:

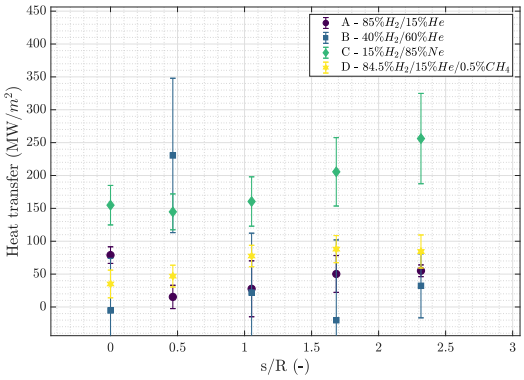

Figure 10: Model heat transfer normalised by s/R

$$q_{conv} = 0.487K\sqrt{\frac{\rho_\infty}{R_n}}U_\infty^3$$

Where K is a gas constant, ρ_∞ is the freestream density, R_n is the sub-scale vehicle nose radius, and U_∞ is the flight equivalent velocity. Values for density were taken from Table 4 with K calculated based on the H_2 mass fraction of interest.

Table 5: Summary of test time averaged stagnation point heat flux versus Sutton and Graves prediction

Condition	K [-]	S&G [MW/m^2]	Experiment [MW/m^2]	Δ [%]
A	1.38e-4	29.4	78.9	168
B	1.88e-4	44.9	-5.3 *	-88
C	4.19e-4	154.2	154.9	1.3
D	1.40e-4	27.3	35.0	28
D †	1.40e-4	27.3	27.4	0.3

* Measurement affected by likely diaphragm fragment impact
† With SiO_2 coating

In an effort to rule minimise potentially ionisation effects from the test gas on the thermocouples a silicon dioxide coating was applied to the model surface. Silicon dioxide with a purity of 99.99% was evaporatively applied to the model surface by the Oxford Thin Film Facility using a Leybold 560 box coater. The film thickness applied was between 700 and 800 nm.

Figure 12 shows a comparison between normalised average heat transfer for two runs of condition D with and without SiO_2 coating. The average heat transfer was within uncertainty for the first two sensors but diverged further along the model surface. The heat flux measured at the stagnation point was still lower than that downstream, but shows good agreement with the value predicted by Sutton & Graves. The magnitude of the 'dip' in the thermocouple traces for the coated case was smaller, meaning that a thicker coating may yield improved results.

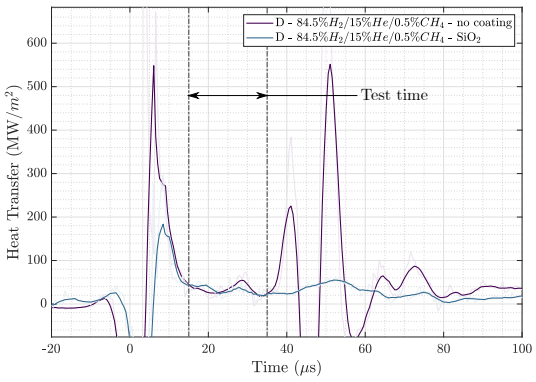

Figure 11: Comparison between stagnation point heat flux traces for the coated and uncoated cases

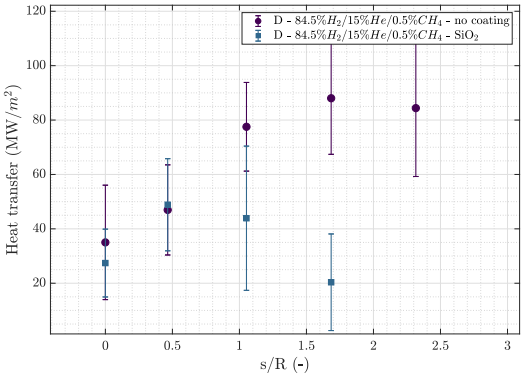

Figure 12: Comparison between normalised average heat transfer for the coated and uncoated cases

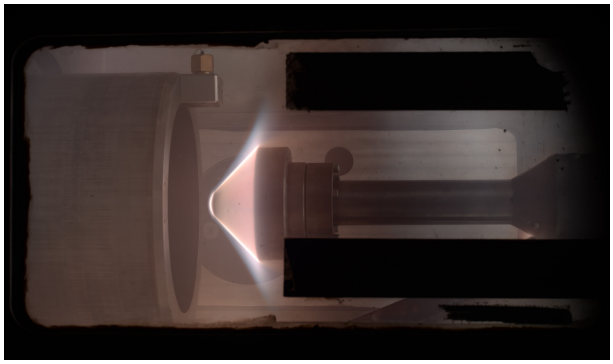

Figure 13: Single frame colour exposure during the test time, captured with the Nikon D610 DSLR camera

Selected frames from the high speed video obtained with the Kirana are shown in Figure 14. The exposure times were 200, 100, 100, and 100 ns respectively with 100 ns being the lowest possible exposure time permitted by the camera. The images in Figure 14 are unfiltered i.e. no bandpass filter was installed. Despite the very low exposure times, the sensor saturated for every shot, however this footage was still useful for verification of accelerator and test gas arrival. In an attempt to prevent the camera sensor from saturating, a 656 nm bandpass filter was installed in front of the camera lens, still with an exposure time of 100 ns. Two shots, T6s349 and T6s350 were run with this setup, both condition D. In these tests, no radiance was visible during the test time. [14] found that relatively high exposure times were required to capture the full extent of the shock layer for gas giant conditions due to the large non-equilibrium region, even due to the point of saturating the camera in the near body equilibrium region. Future experiments to measure the shock stand-off distance should explore the most appropriate camera settings and optical path to achieve the desired effect, possibly utilising a neutral density filter as was done for the DSLR camera.

Figure 13 shows a colour image obtained with the DSLR during the test time for condition D. Initially, this camera was triggered by the data acquisition system with the exposure time set to the minimum possible of 250 µs. It was soon found that the camera had a shutter delay of approximately 54 ms that prohibited accurate triggering from the DAQ. In later shots, the camera was set to 'bulb' exposure mode where the shutter is opened and closed manually. The shutter was opened immediately before the shot and closed immediately after from the control room. This method had the disadvantage of capturing light from the accelerator and driver gas as well as the test gas, however it was sufficient given that the images were not intended for use in quantitative analysis. The camera aperture was set to f22, the smallest possible, and a neutral density filter of optical density 2.0 was setup in front of the lens to limit the amount of light reaching the camera sensor.

5. FUTURE WORK

5.1. Grounding Techniques

In all tests, the baseline noise before the shock wave arrived at the model was small, indicating that the noise was due to an interaction of the test gas with the model and associated instrumentation circuits. All thermocouple traces were characterised by an initial 'dip' in voltage followed by a jump to what might be considered a reasonable value during the test time. The end of the test time was marked by another dip in voltage before arrival of the driver gas.

Palmer [32] performed a series of experiments with thin-film calorimeters in the X1 expansion tube and observed similar features. To avoid risking damage to sensors during noise diagnositic experiments a 5 Ω resistor, chosen to match the thermocouple junction resistance, was placed inside the model and not exposed to the flow. Any deviation from a null signal produced by the resistor circuit could therefore be attributed to solely to electrical interference. Palmer suggested that the noise could be due to a number of effects, including:

1. Induction of electromagnetic effects in the instrumentation
2. The gas acting as a conductor that connects sensors to parts of the facility which may be at slightly different earth potentials to the signal circuit
3. Formation of a plasma sheath (Debye sheath) over the surface of the model leading to a net negative charge at the model surface

Future experimental campaigns with models at Ice Giant entry conditions could benefit from implementation of these techniques.

5.2. Spectroscopy of shock layer and Stalker substitution.

Investigation of the radiative heating environment in the stagnation region via spectroscopy would provide insight into the effect of trace gases on the total heat flux. This has been employed successfully at the University of Queensland on a number of occasions [14]. Additionally, use of this technique would aid in the design of Stalker substituted test conditions since a key requirement for similarity is matching of dissociation/relaxation rates of species (i.e. H-α, H-β).

6. CONCLUSION

A summary of a prelimnary study of a Galieo sub-scale model at Ice Giant entry conditions has been presented. Test flows with flight equivalent velocities of greater than 18 km/s were produced with test times on the order of 30 µs. Heat flux and pressure measurements on the model surface were obtained, however the data indicate that heat flux measurements are affected by electrical interference that was not resolved by initial attempts to isolate the model from the flow. Future experiments should focus on resolving this issue.

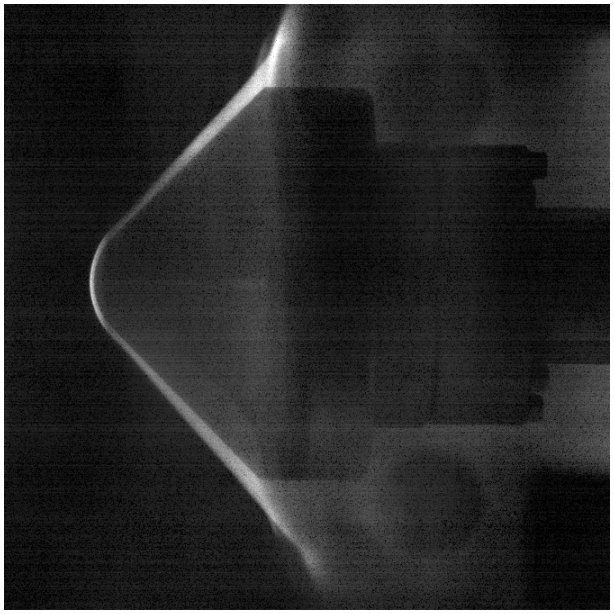

(a) Condition A

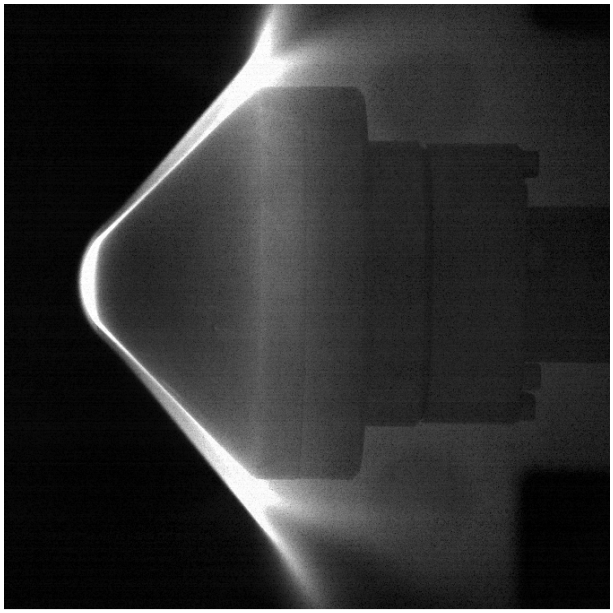

(b) Condition B

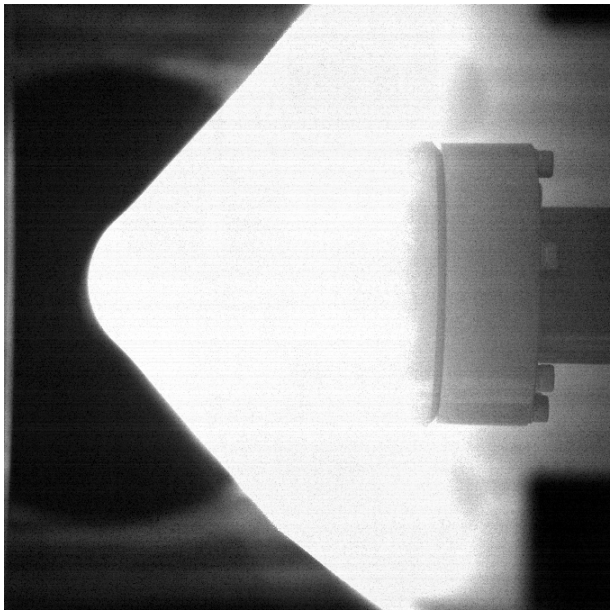

(c) Condition C

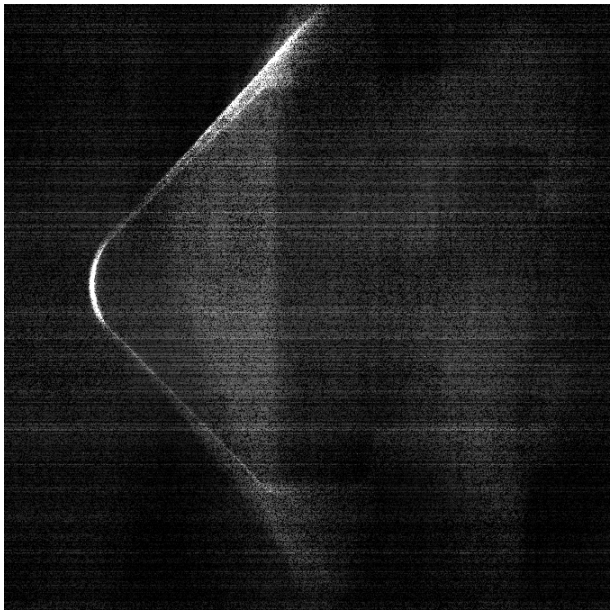

(d) Condition D

Figure 14: Selected single frames from high speed video of the test time

ACKNOWLEDGMENTS

This work is funded within an ESA initiative under contract No. 4000132571/20/NL/MG/rk. We thank the colleagues of the research team in Stuttgart and Oxford. We would also like to acknowledge the building services and workshop staff at the Southwell Building, Millbrook Precision Ltd, and the Oxford Thin Film Facility, without whom this work would certainly not have been possible.

REFERENCES

[1] O. Mousis, D.H. Atkinson, T. Cavalié, L.N. Fletcher, M.J. Amato, S. Aslam, F. Ferri, J.-B. Renard, T. Spilker, E. Venkatapathy, P. Wurz, K. Aplin, A. Coustenis, M. Deleuil, M. Dobrijevic, T. Fouchet, T. Guillot, P. Hartogh, T. Hewagama, M.D. Hofstadter, V. Hue, R. Hueso, J.-P. Lebreton, E. Lellouch, J. Moses, G.S. Orton, J.C. Pearl, A. Sánchez-Lavega, A. Simon, O. Venot, J.H. Waite, R.K. Achterberg, S. Atreya, F. Billebaud, M. Blanc, F. Borget, B. Brugger, S. Charnoz, T. Chiavassa, V. Cottini, L. d'Hendecourt, G. Danger, T. Encrenaz, N.J.P. Gorius, L. Jorda, B. Marty, R. Moreno, A. Morse, C. Nixon, K. Reh, T. Ronnet, F.-X. Schmider, S. Sheridan, C. Sotin, P. Vernazza, and G.L. Villanueva. Scientific rationale for Uranus and Neptune in situ explorations. *Planetary and Space Science*, 155:12–40, June 2018.

[2] Mark Hofstadter, Amy Simon, Sushil Atreya, Donald Banfield, Jonathan J. Fortney, Alexander Hayes, Matthew Hedman, George Hospodarsky, Kathleen Mandt, Adam Masters, Mark Showalter, Krista M. Soderlund, Diego Turrini, Elizabeth Turtle, Kim Reh, John Elliott, Nitin Arora, and Anastassios Petropoulos. Uranus and Neptune missions: A study in advance of the next Planetary Science Decadal Survey. *Planetary and Space Science*, 177:104680, November 2019.

[3] S Bayon. CDF Study Report - Ice Giants. page 431, 2019.

[4] Committee on the Planetary Science and Astrobiology Decadal Survey, Space Studies Board, Division on Engineering and Physical Sciences, and National Academies of Sciences, Engineering, and Medicine. *Origins, Worlds, and Life: A Decadal Strategy for Planetary Science and Astrobiology 2023-2032*. National Academies Press, Washington, D.C., 2022. Pages: 26522.

[5] Michael E. Tauber. Atmospheric entry into Jupiter. *Journal of Spacecraft and Rockets*, 6(10):1103–1109, October 1969.

[6] Peter L Collen, Luke J Doherty, Suria D Subiah, Andrew Hyslop, and Matthew McGilvray. Performance Capability Experiments in T6: A Multi-Mode Ground Test Facility for High-Enthalpy, Aerothermodynamics Research. page 8, 2019.

[7] Matthew McGilvray, Peter Collen, Luke Doherty, Joseph Steer, James Leader, Alex Glenn, and Chris Hambidge. The Oxford T6 Stalker tunnel: performance, upgrades and new modes of operation. 2022. Publisher: European Space Agency.

[8] Frank S. Milos. Galileo Probe Heat Shield Ablation Experiment. *Journal of Spacecraft and Rockets*, 34(6):705–713, November 1997.

[9] Shingo Matsuyama, Naofumi Ohnishi, Akihiro Sasoh, and Keisuke Sawada. Numerical Simulation of Galileo Probe Entry Flowfield with Radiation and Ablation. *Journal of Thermophysics and Heat Transfer*, 19(1):28–35, January 2005.

[10] Chul Park. Stagnation-Region Heating Environment of the Galileo Probe. *Journal of Thermophysics and Heat Transfer*, 23(3):417–424, July 2009.

[11] Grant Palmer, Dinesh Prabhu, and Brett A. Cruden. Aeroheating Uncertainties in Uranus and Saturn Entries by the Monte Carlo Method. *Journal of Spacecraft and Rockets*, 51(3):801–814, May 2014.

[12] Brett A. Cruden and David W. Bogdanoff. Shock Radiation Tests for Saturn and Uranus Entry Probes. *Journal of Spacecraft and Rockets*, 54(6):1246–1257, November 2017.

[13] Christopher M. James, David E. Gildfind, Richard G. Morgan, Steven W. Lewis, and Timothy J. McIntyre. Experimentally Simulating Giant Planet Entry in an Expansion Tube. *Journal of Spacecraft and Rockets*, 57(4):656–671, July 2020.

[14] Yu Liu, Christopher M. James, Richard G. Morgan, and Timothy J. McIntyre. Experimental validation of a test gas substitution for simulating non-equilibrium giant planet entry conditions in impulse facilities. *Experiments in Fluids*, 61(9):198, September 2020.

[15] R. J. Stalker. Shock tunnel measurement of ionization rates in hydrogen. *AIAA Journal*, 18(4):478–480, April 1980.

[16] R. Stalker. A similarity transformation for blunt body flows. In *24th Aerospace Sciences Meeting*, Reno,NV,U.S.A., January 1986. American Institute of Aeronautics and Astronautics.

[17] R. J. Stalker and B. P. Edwards. Hypersonic Blunt-Body Flows in Hydrogen-Neon Mixtures. *Journal of Spacecraft and Rockets*, 35(6):729–735, November 1998.

[18] J. I. Moses, T. Cavalié, L. N. Fletcher, and M. T. Roman. Atmospheric chemistry on Uranus and Neptune. *Philosophical Transactions of the Royal Society A: Mathematical, Physical and Engineering Sciences*, 378(2187):20190477, December 2020.

[19] João Alexandre Abreu Coelho. Aerothermodynamic Analysis of Aerocapture and Ballistic Entry Flows in Neptune's Atmosphere. page 134, 2021.

[20] A. M. Brandis, D. A. Saunders, C. O. Johnston, B. A. Cruden, and T. R. White. Radiative Heating on the After-Body of Martian Entry Vehicles. *Journal of Thermophysics and Heat Transfer*, 34(1):66–77, January 2020.

[21] George R. Inger, Charlotte Higgins, and Richard Morgan. Generalized Nonequilibrium Binary Scaling for Shock Standoff on Hypersonic Blunt Bodies. *Journal of Thermophysics and Heat Transfer*, 17(1):126–128, January 2003.

[22] Guerric De Crombrugghe. *On binary scaling and ground-to-flight extrapolation in high-enthalpy facilities*. PhD Thesis, The University of Queensland, March 2017.

[23] Andreas Andrianatos, David Gildfind, and Richard Morgan. A Study of Radiation Scaling of High Enthalpy Flows in Expansion Tubes. page 14, 2015.

[24] Peter Collen, Luke J Doherty, D Subiah, Tamara Sopek, David Gildfind, Rowland Penty, Rowan Gollan, and Richard Morgan. Development and Commissioning of the T6 Stalker Tunnel. page 41, 2021.

[25] Robert L Trimpi. A preliminary theoretical study of the expansion tube, a new device for producing high-enthalpy short-duration hypersonic gas flows/ by Robert L. Trimpi. page 1, 1962.

[26] Michael P Scott. *Development and Modelling of Expansion Tubes*. PhD thesis, 2006.

[27] C. M. James, D. E. Gildfind, S. W. Lewis, R. G. Morgan, and F. Zander. Implementation of a state-to-state analytical framework for the calculation of expansion tube flow properties. *Shock Waves*, 28(2):349–377, March 2018.

[28] Christopher M. James, David E. Gildfind, Richard G. Morgan, Steven W. Lewis, and Timothy J. McIntyre. Simulating Gas Giant Atmospheric Entry Using Helium and Neon Test Gas Substitutions. *Journal of Spacecraft and Rockets*, 56(3):725–743, May 2019.

[29] MLG Oldfield. Impulse response processing of transient heat transfer gauge signals. 2008.

[30] David R. Buttsworth. Assessment of effective thermal product of surface junction thermocouples on millisecond and microsecond time scales. *Experimental Thermal and Fluid Science*, 25(6):409–420, December 2001.

[31] Kenneth Sutton and Randokh A Graues. A general stagnation-point convective-heating equation for arbitrary gas mixtures. page 67.

[32] Robert A Palmer. Measurement of heat transfer in superorbital flows. 2000.